NANO LETTERS

Letter

pubs.acs.org/NanoLett

Imaging Electrogenerated Chemiluminescence at Single Gold Nanowire Electrodes

Andrew J. Wilson,[†,‡] Kyle Marchuk,[†,‡] and Katherine A. Willets*[,†,‡]

[†]Department of Chemistry, Temple University, Philadelphia, Pennsylvania 19122, United States

[‡]Department of Chemistry, The University of Texas at Austin, Austin, Texas 78712, United States

Supporting Information

ABSTRACT: We report electrogenerated chemiluminescence (ECL) generated at single gold nanowire electrodes supported on tin-doped indium oxide. Unlike other single nanoparticle electrochemical characterization techniques, ECL provides a massively parallel direct readout of electrochemical activity on individual nanoparticle electrodes without the need for extrinsic illumination or a scanning electrochemical probe. While ECL is not observed from as-purchased nanowires due to the surfactant layer, by removing the layer and coating the nanowires with a polymer blend, ECL from single nanowire electrodes is readily measured. With an increase in polymer thickness, an increase in ECL image quality and reproducibility over multiple redox cycles is observed. The polymer coating also provides a strategy for stabilizing gold nanoparticle electrodes against complete surface oxidation in aqueous environments.

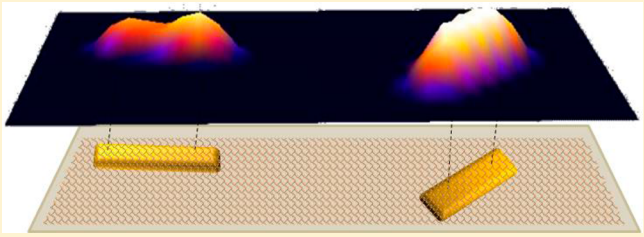

KEYWORDS: *Electrogenerated chemiluminescence, electrochemistry, plasmonics, nanowires, nanoparticle electrode*

Plasmonic nanostructures are increasingly being used as electrodes in electrochemical experiments because their nanoscale features and unique optical properties can increase the efficiency, yield, and selectivity of reactions of interest.[1−9] Utilizing single nanocrystals in electrochemical experiments can allow for greater control and selectivity in electrocatalysis,[10,11] and provide insight into single-molecule electrochemistry,[12,13] yet there are significant challenges to overcome when using nanoparticles as electrodes.[14] For example, synthetic nanoparticles are often prepared using bulky organic ligands that consequently impede electrochemical activity.[15] Moreover, new electrochemical constraints such as size-dependent oxidation potentials[16,17] and extreme sensitivity to surface oxide formation[18] emerge as noble metal electrodes are shrunk to nanoscale dimensions. These considerations severely limit the number of repeat measurements when using nanoparticles as electrodes. Performing reproducible measurements on electrochemically stable metal nanoparticle electrodes is a significant challenge and paramount to the incorporation of these materials into nanoscale electrical systems.

Another challenge when studying electrochemistry on metal nanoparticle electrodes is measuring a redox response from the small number of molecules and electrons interacting with a nanoelectrode. Many experiments overcome this limitation by using nanoparticle arrays to generate a measurable current response.[16,17,19−22] However, it is well-known that the optical properties of plasmonic nanoparticles have extreme sensitivity to their shape and size, and it is important to discover whether similar heterogeneity exists for the electrochemical properties of these materials when used as nanoscale electrodes. To understand this, we require techniques that can probe the electrochemical properties of single nanoparticle electrodes, one at a time. Scanning electrochemical microscopy (SECM) allows for electrochemical measurements on single nanoparticles[23−26] but is time-consuming, sensitive to probe fabrication[27,28] and alignment,[29] and does not allow for many individual nanoparticles to be probed in tandem. Optical techniques, such as fluorescence[30−32] and surface-enhanced Raman scattering (SERS),[12,13] have also been used to interrogate electrochemistry on single nanoparticle electrodes by measuring changes in the optical signatures of probe molecules upon oxidation and reduction. These strategies require the use of an extrinsic illumination source, which may bias electrochemical measurements through local heating of the electrode surface or (in the case of plasmonic nanoparticle electrodes) plasmon-mediated hot electron production.[1,33,34] Moreover, the probe molecules are susceptible to photobleaching at high laser intensities, which makes it difficult to discriminate loss of signal due to probe degradation versus nanoparticle damage/oxidation over multiple redox cycles.

As an alternative approach, electrogenerated chemiluminescence (ECL) provides the opportunity to take advantage of the sensitivity of an optical readout of electrochemical activity without the use of an illumination source or the need of a scanning probe technique.[35,36] ECL has been used to study micron-sized particles[37,38] and arrays of nanoparticles[39,40] but has not been reported on individual noble metal nanoparticle electrodes. ECL microscopy has the potential to provide a rapid

Received: June 16, 2015
Revised: August 4, 2015
Published: August 12, 2015

DOI: 10.1021/acs.nanolett.5b02383
Nano Lett. 2015, 15, 6110−6115

and robust method to study how individual nanoparticle shape, size, and composition influence electrochemical activity at the nanoscale. In this Letter, we use ECL as an optical readout of electrochemical activity at the single nanoparticle level, a measurement not readily achievable with conventional electrochemical methods.

The experiments herein show ECL from the tris(2,2′-bipyridyl)dichlororuthenium(II) ($Ru(bpy)_3^{2+}$) and tripropylamine (TPA) coreactant pair[41] at single gold nanowire electrodes. Reproducible ECL is achieved by partially removing the hexadecyltrimethylammonium surfactant (CTA^+) from the purchased gold nanowires (Nanopartz) and subsequently coating them with a polymer blend consisting of poly(3,4-ethylenedioxythiophene)−poly(styrenesulfonate) (PEDOT:PSS) and poly(vinyl alcohol) (PVA). Gold nanowires are drop-cast onto a tin-doped indium oxide (ITO)-coated microscope coverslip to serve as a working electrode, and platinum and Ag/AgCl wires are used for auxiliary and reference electrodes, respectively. Our electrochemical cells are fabricated to be compatible with an Olympus IX73 inverted microscope equipped with an Olympus U-DCD dark-field condenser and a Princeton Instruments PhotonMAX EM-CCD detector (see Supporting Information for details, Figure S1). To produce ECL, the potential is held at 0 V for 5 s and stepped to +1.2 V for 2 s in a solution of 1 mM $Ru(bpy)_3^{2+}$, 10 mM TPA, and 0.25 M phosphate buffer at pH 7.2. Additional experimental details can be found in the Supporting Information.

Figure 1 compares the dark-field microscopy images of gold nanowires with different surface treatments and the resulting $Ru(bpy)_3^{2+*}$ (emissive form of $Ru(bpy)_3^{2+}$) ECL image. A sample prepared by drop casting as-purchased gold nanowires onto an ITO-coated glass coverslip is shown in Figure 1, panels A and B. No ECL was recorded for this sample. A CTA^+ bilayer exists on the nanowire surface as a consequence of synthesis,[42] and the lack of ECL suggests that the bulky stabilizing ligand bilayer blocks electron transfer and prevents ECL. To test this hypothesis, we prepared a sample by drop casting gold nanowires on an ITO-coated glass coverslip followed by placing the sample in boiling water for 1 h. This treatment is sufficient to perturb the bilayer and solvate some of the CTA^+ ligands, leaving an exposed gold surface.[43] Figure 1, panels C and D show that ligand removal allows ECL to be produced at the nanowire surface. Importantly, the ECL produced at the gold nanowire electrodes has a significantly higher intensity contrast relative to ECL at the supporting ITO electrode, allowing us to discriminate ECL at the nanoparticles from ECL at the substrate (Supporting Information, Figures S2, S3, and S5).[40,44] While the strategy of removing CTA^+ allows for the imaging of ECL from single nanowire electrodes on a microscope, the nanowires quickly become electrochemically inactive, most likely due to the formation of a gold surface oxide, resulting in the loss of ECL signal (Figure S6 and discussion below).

To preserve the exposed surfaces of the gold nanowires on ITO after partial CTA^+ removal, we coat the nanowires with a polymer film prepared from a solution of 15% (v/v) PEDOT:PSS in a 3% PVA solution. PEDOT:PSS was chosen due to it being both electrically conductive and optically transparent, while PVA gives the polymer blend mechanical strength and provides strong adhesion to the substrate.[45,46] The PSS in the PEDOT:PSS−PVA blend readily takes up cations, allowing us to preload the film by incubation in a 1 mM

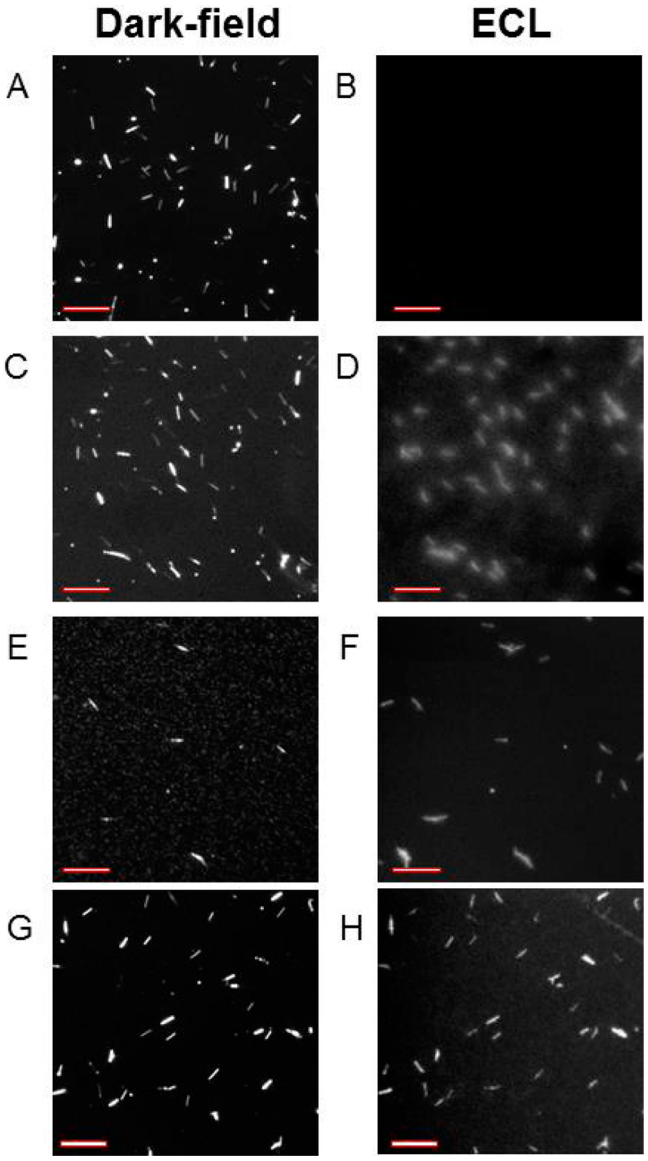

Figure 1. (left column) Dark-field scattering images of single gold nanowires electrodes and (right column) the corresponding $Ru(bpy)_3^{2+*}$ ECL produced at each nanowire when the potential was held at +1.2 V. (A, B) As-purchased gold nanowires on ITO; (C, D) gold nanowires on ITO boiled in water to remove surfactant; (E-H) gold nanowires on ITO, boiled in water, and coated with PEDOT:PSS−PVA by (E, F) drop casting and (G, H) spin coating at 1000 rpm. Samples coated with PEDOT:PSS−PVA were incubated in 1 mM $Ru(bpy)_3^{2+}$ for 1 h prior to electrochemical measurements. All samples were immersed in a solution of 1 mM $Ru(bpy)_3^{2+}$, 10 mM TPA, and 0.25 M phosphate buffer at pH 7.2. Scale bars are 20 μm.

$Ru(bpy)_3^{2+}$ solution for 1 h prior to electrochemical measurements.[47] With the partially exposed nanowires coated with this polymer blend, ECL can easily be observed over the ITO background in Figure 1, panel F (drop-cast polymer film) and Figure 1, panel H (spin coated polymer film). Moreover, because the $Ru(bpy)_3^{2+}$ is captured by the polymer coating, the ECL images look much sharper in comparison to the image in Figure 1, panel D, where the $Ru(bpy)_3^{2+*}$ diffuses away from the nanowire surface creating a blurred-looking image. It is important to note that in comparing Figure 1, panels E and F, in which the polymer film is introduced via drop casting, there appear to be more particles in the ECL image than in the dark-

DOI: 10.1021/acs.nanolett.5b02383
Nano Lett. 2015, 15, 6110−6115

field image. This is due to the optical extinction of the polymer film at thicknesses (~5−10 μm) created by drop casting, which reduces the scattering contrast in the dark-field measurement. Bright-field imaging allows additional ECL emission centers to be colocalized with nanowires at these nonscattering regions (Figure S7). However, we still find that ~25% of the ECL emission centers cannot be colocalized with nanowires observed with either dark- or bright-field imaging due to reduced contrast produced by the microns-thick drop-cast polymer film. Thus, ECL provides a mechanism for us to identify electrochemically active nanowires in the thick film that are not observable using bright- or dark-field imaging.

In the case when the nanowires are covered with a spin-coated film (Figure 1G,H), the thinner film (~300 nm) has a lower optical extinction compared to the drop-cast film and allows us to readily observe dark-field scattering from the nanowires (Figure 1G). Here we find that several nanowires that are present in the dark-field image are not observed in the associated ECL image (Figure 1H), which suggests that these nanowires either have poor electrochemical contact with the ITO or have had an insufficient amount of the CTA^+ ligand removed. For all samples investigated (149 nanowires), 82.5% of nanowires were visible with both dark-/bright-field and ECL imaging, 7.4% of nanowires were visible with dark-/bright-field and not with ECL imaging, and 10.1% were visible with ECL imaging and not with dark-/bright-field imaging.

An important result of coating the gold nanowire electrodes with PEDOT:PSS−PVA is the reproducibility of our electrochemical measurements. Figure 2 shows the applied potential

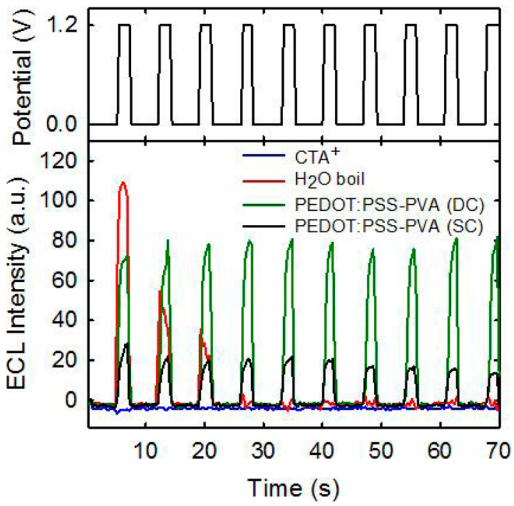

Figure 2. Applied potential waveform and integrated ECL intensity-time traces of a single CTA^+ coated nanowire (blue), a partially coated CTA^+ nanowire boiled in H_2O (red), and nanowires coated with $Ru(bpy)_3^{2+}$-doped PEDOT:PSS−PVA by drop casting (DC) (green) and spin coating (SC) at 1000 rpm (black). All samples were immersed in a solution of 1 mM $Ru(bpy)_3^{2+}$, 10 mM TPA, and 0.25 M phosphate buffer at pH 7.2.

waveform and the background subtracted ECL intensity trajectories at single gold nanowires over 10 potential cycles. As previously stated, and shown with the blue intensity trajectory in Figure 2, no ECL is observed from the as-purchased nanowires without removing CTA^+. With partial removal of CTA^+, a strong ECL signal is initially measured, followed by intensity decay with each successive potential cycle until the signal goes to background (Figure 2, red trajectory). It is well-known that surface oxidation will quickly and irreversibly cover the exposed gold at the applied anodic potentials, leading to loss of ECL signals, although other factors such as ligand rearrangement and impurity passivation must also be considered.[48,49] To test the role of surface oxide formation, repeated cyclic voltammetry experiments were performed on the $Ru(bpy)_3^{2+}$/TPA system using a bulk gold disc electrode and showed that a surface oxide grows on the bare gold electrode with each potential cycle, causing a decrease in the anodic current associated with ECL (Figure S6). The decrease in anodic current on a bulk disc electrode with each potential cycle matches the trend of ECL signal decrease on the bare nanowires, supporting oxide formation as the cause for ECL loss. While surface oxide formation is straightforward to measure on a bulk electrode surface using cyclic voltammetry, characterizing loss of electrochemical activity on single gold nanowires is much more challenging, especially in real time and on multiple nanowires in tandem. Common single nanoparticle characterization techniques, such as dark-field scattering and scanning electron microscopy (Figures S8 and S9, respectively), provide no clue that electrochemical oxidation has occurred on the nanowire surface, highlighting the power of ECL for providing a rapid and accurate readout of nanowire electrode stability over multiple potential cycles.

The green ECL intensity trajectory in Figure 2 shows that nanowires coated with PEDOT:PSS−PVA by drop casting give much improved electrochemical stability, demonstrated by the ECL signal remaining consistent over all 10 potential cycles (additional examples shown in Figure S10). Spin coating PEDOT:PSS−PVA on the nanowires also improves electrochemical stability, as shown by the black ECL trajectory in Figure 2, although the overall signal is lower. To test whether the polymer blend is providing protection against surface oxide formation, we again performed repeated cyclic voltammetry experiments on the $Ru(bpy)_3^{2+}$/TPA system using a bulk gold disc electrode coated with both PVA alone and the PEDOT:PSS−PVA blend (Figure S6). In both cases, we observe a decrease in the current associated with gold oxide reduction, suggesting that the protective polymer film significantly retards the formation of a surface oxide on the gold surface. Moreover, the anodic current associated with $Ru(bpy)_3^{2+}$ and TPA oxidation remains stable over multiple potential scans, consistent with the ECL results observed optically on the gold nanowires (Figure 2). The bulk voltammetry data in Figure S6 also show increased current from $Ru(bpy)_3^{2+}$ and TPA oxidation when PEDOT:PSS is introduced into the PVA matrix, suggesting that the charged polymer concentrates the electro-active species near the electrode surface. Thus, the combination of the charged PEDOT:PSS polymer with the mechanically stable PVA provides both enhanced protection of the gold surface against oxide formation as well as increased signals from the cationic ECL probes.

In the earlier examples, the PEDOT:PSS−PVA films were preloaded with the $Ru(bpy)_3^{2+}$ by incubating the films in a 1 mM solution for 1 h. However, by using ECL as a readout, we are able to track the loading process, as shown in Figure 3. Here, an undoped 300 nm PEDOT:PSS−PVA film was spin-cast on top of the partially exposed gold nanowires, and then the sample was placed on the microscope and exposed to a solution of 1 mM $Ru(bpy)_3^{2+}$ and 10 mM TPA in 0.25 M phosphate buffer at pH 7.2. Potential steps of +1.2 V were applied several times over the course of the 70 min experiment,

DOI: 10.1021/acs.nanolett.5b02383
Nano Lett. 2015, 15, 6110−6115

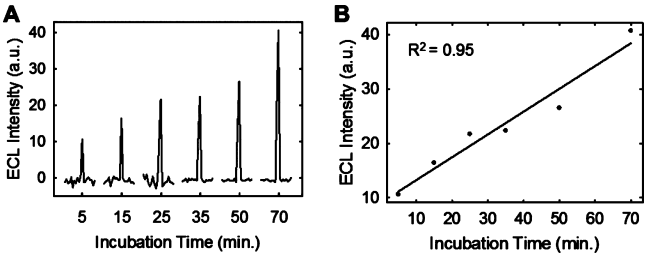

Figure 3. Integrated ECL intensity at a single gold nanowire electrode coated with 300 nm of undoped PEDOT:PSS−PVA as a function of incubation time in a solution of 0.25 M phosphate buffer at pH 7.2, 10 mM TPA, and 1 mM $Ru(bpy)_3^{2+}$. (A) ECL signal generated at +1.2 V for 2 s at select incubation times. (B) Maximum ECL intensity and best fit line showing a linear increase in signal with incubation time.

and each time, the measured ECL signal at a single gold nanowire electrode increased, as shown in Figure 3, panel A. The plot of the peak intensity as a function of incubation time shows a linear rise in intensity (Figure 3B). Importantly, even after 5 min, we are able to obtain strong ECL signal, indicating that the $Ru(bpy)_3^{2+}$ and TPA can rapidly diffuse from solution through the porous polymer film and be oxidized at the gold nanowire surface. Thus, the polymer blend is able to protect the gold nanowire against electrochemical damage while still allowing cations to quickly reach the electrode surface. Full saturation of the polymer film takes several hours (Figure S11), yet high dye loading is achievable at relatively short incubation times.

Next, we investigated the effect that the thickness of the polymer coating has on imaging ECL. To vary the thickness of PEDOT:PSS−PVA, we spin coated the polymer blend at 4000, 2000, and 1000 rpm for film thicknesses of 70, 120, and 300 nm, respectively. Atomic force microscopy was used to approximate the film thickness by scratching off a small area of polymer. Figure 4, panel A shows that a polymer layer of 70 nm produces a blurry ECL image, which makes it difficult to resolve individual nanowires and requires comparison with dark-field images to assign signals to specific nanowire electrodes (Figure S12). Increasing the polymer thickness to 120 nm gives a sharper ECL image of the nanowire electrodes but still includes a haze around the nanowires, as shown in Figure 4, panel B. In contrast, a 300 nm film gives a clear, sharp image of ECL at the nanowires (Figure 4C). Cross-sections of the ECL emission profile across the width of the nanowires show that sharper ECL images are produced with thicker polymer films over the nanowires (Figure S13). The reason for the blurry ECL images from the 70 and 120 nm films can be explained by considering several possible mechanisms. First, in thin films, the excited $Ru(bpy)_3^{2+*}$ may escape more quickly from the polymer matrix into bulk solution where its diffusion will be faster, resulting in a blurred ECL image. As the film thickness increases, the $Ru(bpy)_3^{2+*}$ dwells longer in the polymer, where its diffusion is slower, and we obtain a sharper overall image. To verify this, we compared the ECL cross-sections for several bare nanowires from Figure 1, panel D to the polymer-coated wires from Figure 4; interestingly, we observe that the ECL cross-sections are comparable or even somewhat larger for the nanowires coated with the 70 nm polymer film than the bare nanowires, which suggests that the polymer could also be contributing to the blurred appearance of the ECL from the nanowire electrodes. One possibility is that as the polymer film becomes thinner, the diffusion profile transitions from radial to lateral, blurring the image. A second possibility is that the excited state lifetime of $Ru(bpy)_3^{2+*}$ may be longer in the polymer film than in free solution,[50,51] so we are able to observe molecules farther from the nanowire surface, in contrast to the polymer-free examples in Figure 1, panel D. Although we cannot differentiate between these different mechanisms (and multiple mechanisms may be simultaneously in play), the optimal condition for obtaining sharp ECL images of nanowire electrodes is by coating them with a thick polymer film.

PEDOT:PSS−PVA film thickness is also important to consider for the reproducibility of the electrochemical measurements. Figure 5 compares the ECL signal measured over 10 potential step cycles for different film thicknesses. Each film was doped with $Ru(bpy)_3^{2+}$ by incubation with a 1 mM $Ru(bpy)_3^{2+}$ solution for 1 h prior to the electrochemical measurements. The red ECL trajectory in Figure 5 shows that the 70 nm polymer film initially gave a strong ECL signal followed by a rapidly decaying intensity profile with each successive potential cycle. Similarly, the 300 nm film (black trajectory, Figure 5) shows decay in the ECL signal with successive potential cycles, albeit at a slower rate than the thinner film. By using this trend, and with the goal of generating consistent ECL signals for many cycles, we created a thick polymer film (5−10 μm) by drop casting. Although this type of film does not have a well-controlled thickness, the green ECL trajectory in Figure 5 shows the drop casting method yields consistent ECL signals over many potential cycles.

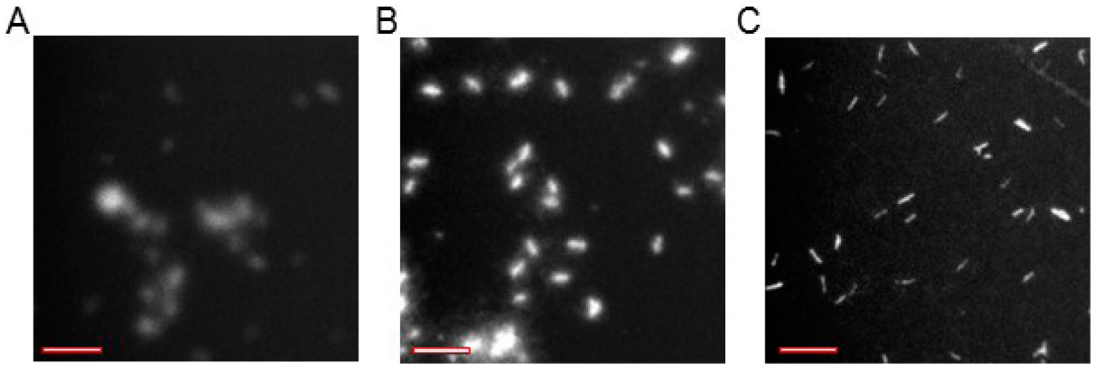

Figure 4. ECL images of gold nanowires coated with $Ru(bpy)_3^{2+}$-doped PEDOT:PSS−PVA of different thicknesses. Polymer film thickness was varied by spin coating to produce films with thicknesses of (A) 70, (B) 120, and (C) 300 nm. Scale bars are 20 μm.

DOI: 10.1021/acs.nanolett.5b02383
Nano Lett. 2015, 15, 6110−6115

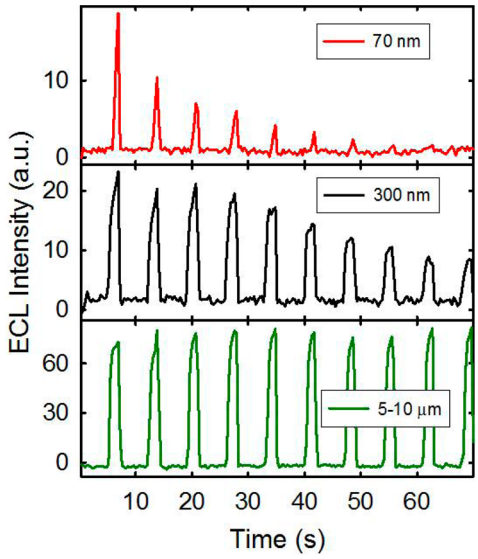

Figure 5. ECL trajectories of individual nanowires coated with a PEDOT:PSS−PVA film at thickness of 70 nm (4000 rpm, red curve), 300 nm (1000 rpm, black curve), and 5−10 μm (drop casting, green curve). As the film thickness increases, the reproducibility of the ECL signals over 10 potential cycles increases. All samples were preloaded with $Ru(bpy)_3^{2+}$ and then exposed to a solution of 1 mM $Ru(bpy)_3^{2+}$, 10 mM TPA, and 0.25 M phosphate buffer at pH 7.2. The potential was modulated between 0 V (5 s) and +1.2 V (2 s) for 10 cycles.

To explain the relationship between the decay in the ECL intensity and the polymer film thickness, we first considered the possibility of surface oxide formation on the gold nanowires, similar to the bare nanowire electrodes shown in Figure 2. A thinner film could lead to poorer protection of the gold nanowire surface, leading to faster gold oxidation and more rapid loss of ECL signal. To test this, we looked at ECL intensity time traces of individual nanowires coated with a 300 nm polymer film and incubated in a 1 mM $Ru(bpy)_3^{2+}$ solution for 1 h. Over the first 10 potential cycles, the peak ECL intensity was found to decay linearly, similar to the data shown in Figure 5 (Figure S14). We then allowed the sample to incubate in the solution for an additional 45 min and ran 10 additional potential cycles. In this case, we found that the peak ECL intensity was nearly double the original peak ECL intensity, yet followed a similar linear decay over the 10 applied potential cycles (Figure S14). The rise in ECL intensity after the additional 45 min incubation period indicates that electrode surface oxidation is not the mechanism responsible for the decay in ECL intensity observed in Figure 5. Moreover, doubling of the ECL intensity for this increased incubation time matches well with ECL coreactant loading (Figure S11), suggesting that the time-dependent changes in the ECL intensity are related to the concentration of available analyte rather than an increase in electrode area due to electrochemical roughening. We also note that the increase in ECL intensity occurs only during periods when the potential is off, which further supports our claim that electrode roughening does not occur (see Supporting Information for additional discussion).

Next, we considered the possibility that analyte depletion over the course of the experiment could explain the thickness-dependent intensity loss in Figure 5. To probe this further, we studied the ECL intensity decay from the $Ru(bpy)_3^{2+}$/TPA system using nanowires coated with a 300 nm PEDOT:PSS−PVA film and exposed to three pulse sequences: (1) incubation in 1 mM $Ru(bpy)_3^{2+}$ for 1 h followed by exposure to a 1 mM $Ru(bpy)_3^{2+}$, 10 mM TPA, 0.25 M phosphate buffer solution and applying 10 potential steps between 0 and +1.2 V; (2) 10 additional potential steps taken ∼3 min after sequence 1; and (3) 10 potential steps taken 30 min after sequence 2 (Figures S15 and S16). During sequence 1, the ECL intensity decayed linearly but transitioned to a nonlinear decay reaching a steady state intensity of ∼10% of its initial signal by the end of sequence 2. This constant ECL intensity trend at the end of sequence 2 was reproducible over multiple nanowires (Figure S15) and suggests that the diffusion of the ECL coreactants has reached a steady state, that is, the rate of depletion of reactant(s) is balanced by the infusion of fresh reactants into the polymer film, further supporting the hypothesis that analyte depletion is the main source of ECL intensity loss. Importantly, we also found that between each pulse sequence, the ECL intensity rose, indicating that analyte is replenished during times when no potential was applied to the system. Thus, the analyte-depletion appears to be a potential-dependent phenomenon associated with times when an oxidizing potential is applied (see Supporting Information for additional discussion).

In conclusion, we imaged ECL from $Ru(bpy)_3^{2+*}$ at single gold nanowires by coating them with a protective polymer layer, which both concentrates cationic analytes near the electrode surface and protects the gold from electrochemical damage. Our experiments are the first in which an electrochemical reaction can be directly visualized and followed in real time at a single nanoscale-dimension metal electrode without the need for extrinsic illumination or a scanning probe technique. We are able to confirm that the nanowires are responsible for the observed signals given the excellent agreement between the shape, size, and orientation of the nanowires in the dark-field and ECL images. Moreover, we are able to address individual nanowire electrodes and compile statistics on the number of nanowires that show ECL activity compared to those that are inactive, a measurement that cannot be easily performed with traditional electrochemistry techniques. We have also shown that PEDOT:PSS−PVA, an inexpensive and easily adaptable protective layer, was found to protect nanoparticles from oxidative or other electrochemical damage that typically occurs when electrodes are shrunk to nanoscale dimensions. The polymer thickness affected the sharpness of the ECL images and the reproducibility of ECL intensity over consecutive potential cycles but did not affect the ability of the film to protect the nanowires against oxidative or other damage based on the reproducibility of the ECL signal. Our strategy provides a simple, straightforward means for testing the stability of nanoscale electrodes in various electrochemical environments at the single nanoparticle level and allows for future studies in which the impact of heterogeneity in nanoparticle electrode shape, size, and composition on the electrochemical properties of nearby molecules can be explored.

■ ASSOCIATED CONTENT

Supporting Information

The Supporting Information is available free of charge on the ACS Publications website at DOI: 10.1021/acs.nanolett.5b02383.

DOI: 10.1021/acs.nanolett.5b02383
Nano Lett. 2015, 15, 6110−6115

Sample preparation, experimental setup, cyclic voltammograms, dark-field images, and additional ECL time traces (PDF)

AUTHOR INFORMATION

Corresponding Author

*E-mail: kwillets@temple.edu.

Notes

The authors declare no competing financial interest.

ACKNOWLEDGMENTS

Work was supported by the Department of Energy (DOE), Office of Science, Basic Energy Science (BES) under Award No. DE-SC0010307 (A.J.W.) and the AFOSR MURI Award No. FA9550-14-1-1003 (K.M.), as well as start-up funds from Temple University.

REFERENCES

(1) Mubeen, S.; Lee, J.; Singh, N.; Kramer, S.; Stucky, G. D.; Moskovits, M. *Nat. Nanotechnol.* **2013**, *8*, 247−251.
(2) Berry, C. W.; Wang, N.; Hashemi, M. R.; Unlu, M.; Jarrahi, M. *Nat. Commun.* **2013**, *4*, 1622.
(3) Nishijima, Y.; Ueno, K.; Yokota, Y.; Murakoshi, K.; Misawa, H. *J. Phys. Chem. Lett.* **2010**, *1*, 2031−2036.
(4) Zhang, X.; Wang, P.; Zhang, Z.; Fang, Y.; Sun, M. *Sci. Rep.* **2014**, *4*, 5407.
(5) Sun, M.; Zhang, Z.; Zheng, H.; Xu, H. *Sci. Rep.* **2012**, *2*, 647.
(6) Thimsen, E.; Le Formal, F.; Grätzel, M.; Warren, S. C. *Nano Lett.* **2011**, *11*, 35−43.
(7) Cheng, W.; Dong, S.; Wang, E. *J. Phys. Chem. B* **2004**, *108*, 19146−19154.
(8) Sakai, N.; Fujiwara, Y.; Takahashi, Y.; Tatsuma, T. *ChemPhysChem* **2009**, *10*, 766−769.
(9) Park, J.-E.; Momma, T.; Osaka, T. *Electrochim. Acta* **2007**, *52*, 5914−5923.
(10) Li, Y.; Cox, J. T.; Zhang, B. *J. Am. Chem. Soc.* **2010**, *132*, 3047−3054.
(11) Solla-Gullon, J.; Vidal-Iglesias, F. J.; Lopez-Cudero, A.; Garnier, E.; Feliu, J. M.; Aldaz, A. *Phys. Chem. Chem. Phys.* **2008**, *10*, 3689−3698.
(12) Cortés, E.; Etchegoin, P. G.; Le Ru, E. C.; Fainstein, A.; Vela, M. E.; Salvarezza, R. C. *J. Am. Chem. Soc.* **2010**, *132*, 18034−18037.
(13) Wilson, A. J.; Willets, K. A. *Nano Lett.* **2014**, *14*, 939−945.
(14) Byers, C. P.; Hoener, B. S.; Chang, W.-S.; Yorulmaz, M.; Link, S.; Landes, C. F. *J. Phys. Chem. B* **2014**, *118*, 14047−14055.
(15) Xiao, X.; Pan, S.; Jang, J. S.; Fan, F.-R. F.; Bard, A. J. *J. Phys. Chem. C* **2009**, *113*, 14978−14982.
(16) Ivanova, O. S.; Zamborini, F. P. *J. Am. Chem. Soc.* **2010**, *132*, 70−72.
(17) Ivanova, O. S.; Zamborini, F. P. *Anal. Chem.* **2010**, *82*, 5844−5850.
(18) Brummer, S. B.; Makrides, A. C. *J. Electrochem. Soc.* **1964**, *111*, 1122−1128.
(19) Sibbald, M. S.; Chumanov, G.; Cotton, T. M. *J. Phys. Chem.* **1996**, *100*, 4672−4678.
(20) Campbell, F. W.; Belding, S. R.; Baron, R.; Xiao, L.; Compton, R. G. *J. Phys. Chem. C* **2009**, *113*, 9053−9062.
(21) Shipway, A. N.; Lahav, M.; Blonder, R.; Willner, I. *Chem. Mater.* **1999**, *11*, 13−15.
(22) Nakamoto, K.; Kurita, R.; Niwa, O. *Anal. Chem.* **2012**, *84*, 3187−3191.
(23) Tel-Vered, R.; Bard, A. J. *J. Phys. Chem. B* **2006**, *110*, 25279−25287.
(24) Sánchez-Sánchez, C. M.; Solla-Gullón, J.; Vidal-Iglesias, F. J.; Aldaz, A.; Montiel, V.; Herrero, E. *J. Am. Chem. Soc.* **2010**, *132*, 5622−5624.
(25) Zhang, J.; Lahtinen, R. M.; Kontturi, K.; Unwin, P. R.; Schiffrin, D. J. *Chem. Commun.* **2001**, 1818−1819.
(26) Sun, T.; Yu, Y.; Zacher, B. J.; Mirkin, M. V. *Angew. Chem., Int. Ed.* **2014**, *53*, 14120−14123.
(27) Mirkin, M. V.; Fan, F.-R. F.; Bard, A. J. *Int. J. Devoted Asp. Electrode Kinet. Interfacial Struct. Prop. Electrolytes Colloid Biol. Electrochem.* **1992**, *328*, 47−62.
(28) Sun, P.; Zhang, Z.; Guo, J.; Shao, Y. *Anal. Chem.* **2001**, *73*, 5346−5351.
(29) Shen, M.; Arroyo-Currás, N.; Bard, A. J. *Anal. Chem.* **2011**, *83*, 9082−9085.
(30) Palacios, R. E.; Fan, F.-R. F.; Bard, A. J.; Barbara, P. F. *J. Am. Chem. Soc.* **2006**, *128*, 9028−9029.
(31) Palacios, R. E.; Fan, F.-R. F.; Grey, J. K.; Suk, J.; Bard, A. J.; Barbara, P. F. *Nat. Mater.* **2007**, *6*, 680−685.
(32) Xu, W.; Shen, H.; Kim, Y. J.; Zhou, X.; Liu, G.; Park, J.; Chen, P. *Nano Lett.* **2009**, *9*, 3968−3973.
(33) Mukherjee, S.; Libisch, F.; Large, N.; Neumann, O.; Brown, L. V.; Cheng, J.; Lassiter, J. B.; Carter, E. A.; Nordlander, P.; Halas, N. J. *Nano Lett.* **2013**, *13*, 240−247.
(34) Marchuk, K.; Willets, K. A. *Chem. Phys.* **2014**, *445*, 95−104.
(35) Richter, M. M. *Chem. Rev.* **2004**, *104*, 3003−3036.
(36) Miao, W. *Chem. Rev.* **2008**, *108*, 2506−2553.
(37) Benoist, D. M.; Pan, S. *J. Phys. Chem. C* **2010**, *114*, 1815−1821.
(38) Sentic, M.; Milutinovic, M.; Kanoufi, F.; Manojlovic, D.; Arbault, S.; Sojic, N. *Chem. Sci.* **2014**, *5*, 2568−2572.
(39) Wang, D.; Guo, L.; Huang, R.; Qiu, B.; Lin, Z.; Chen, G. *Sci. Rep.* **2015**, *5*, 7954.
(40) Chen, Z.; Zu, Y. *Langmuir* **2007**, *23*, 11387−11390.
(41) Noffsinger, J. B.; Danielson, N. D. *Anal. Chem.* **1987**, *59*, 865−868.
(42) Nikoobakht, B.; El-Sayed, M. A. *Langmuir* **2001**, *17*, 6368−6374.
(43) Lopez-Sanchez, J. A.; Dimitratos, N.; Hammond, C.; Brett, G. L.; Kesavan, L.; White, S.; Miedziak, P.; Tiruvalam, R.; Jenkins, R. L.; Carley, A. F.; Knight, D.; Kiely, C. J.; Hutchings, G. J. *Nat. Chem.* **2011**, *3*, 551−556.
(44) Fang, L.; Lü, Z.; Wei, H.; Wang, E. *Anal. Chim. Acta* **2008**, *628*, 80−86.
(45) Chen, C.; Torrents, A.; Kulinsky, L.; Nelson, R. D.; Madou, M. J.; Valdevit, L.; LaRue, J. C. *Synth. Met.* **2011**, *161*, 2259−2267.
(46) Carr, O.; Gozzi, G.; Santos, L. F.; Faria, R. M.; Chinaglia, D. L. *Transl. Mater. Res.* **2015**, *2*, 015002.
(47) Sun, C.; Lu, W.; Gao, Y.; Li, J. *Anal. Chim. Acta* **2009**, *632*, 163−167.
(48) Zu, Y.; Bard, A. J. *Anal. Chem.* **2000**, *72*, 3223−3232.
(49) Oesch, U.; Janata, J. *Electrochim. Acta* **1983**, *28*, 1247−1253.
(50) Gryczynski, I.; Malicka, J.; Holder, E.; DiCesare, N.; Lakowicz, J. R. *Chem. Phys. Lett.* **2003**, *372*, 409−414.
(51) Morris, K. J.; Roach, M. S.; Xu, W.; Demas, J. N.; DeGraff, B. A. *Anal. Chem.* **2007**, *79*, 9310−9314.

DOI: 10.1021/acs.nanolett.5b02383
Nano Lett. 2015, 15, 6110−6115